Invited Paper

Ultraviolet detector materials and devices studied by femtosecond nonlinear optical techniques

M. Wraback[a], H. Shen[a], P. Kung[b], M. Razeghi[b], J.C. Carrano[c], T. Li[d], and J.C. Campbell[d]

[a]U.S. Army Research Laboratory, Sensors and Electron Devices Directorate, AMSRL-SE-EM, 2800 Powder Mill Road, Adelphi, MD 20783

[b]Center for Quantum Devices, Department of Electrical and Computer Engineering, Northwestern University, Evanston, IL 60208

[c]Photonics Research Center, Department of Electrical Engineering and Computer Science, U.S. Military Academy, West Point, NY 10996

[d]Microelectronics Research Center, Department of Electrical and Computer Engineering, The University of Texas at Austin, Austin, TX 78712

ABSTRACT

Femtosecond nonlinear optical techniques have been employed in the study of carrier dynamics and transport in ultraviolet detector materials. Visible femtosecond pulses derived from the signal beam of a 250 kHz regenerative amplifier-pumped optical parametric amplifier were frequency doubled to obtain pulses tunable from 250 nm to 375 nm. Time-resolved reflectivity experiments indicate that the room-temperature carrier lifetime in GaN grown by double lateral epitaxial overgrowth (330 ps) is about 3 times longer than that of GaN grown on sapphire without benefit of this technique (130 ps). The electron velocity-field characteristic and saturation velocity in GaN have been obtained from time-resolved studies of electroabsorption in a GaN p-i-n diode. The peak steady-state velocity of 1.9×10^7 cm/s in this device occurs at 225 kV/cm. Time-resolved transmission measurements have been used to monitor ultrafast carrier relaxation phenomena in a thin AlGaN layer with bandgap in the solar blind region of the spectrum. Excitation intensity and wavelength dependent studies of the photoinduced bleaching decays suggest that they are primarily governed by trapping in a high density of sub-bandgap defect levels.

Keywords: femtosecond, time-resolved, reflectivity, transmission, electroabsorption, GaN, AlGaN, lifetime, dynamics, electron velocity

1. INTRODUCTION

Ultraviolet (UV) photodetectors may become important elements in threat warning systems such as visible-blind and solar blind detectors for many military platforms. III-nitride semiconductors have emerged as the materials of choice for these UV applications because of their wide bandgap, high breakdown voltage, large electron saturation velocity, and potential for operation in harsh, high temperature environments. While it is possible to tune the bandgap of $Al_xGa_{1-x}N$ from 365 nm to 200 nm by varying the aluminum content, there is no laser source that is continuously tunable throughout this wavelength range. Moreover, improvement of photodetectors based on GaN and AlGaN will require an understanding of the fundamental scattering, recombination, and transport processes occurring in these devices. These two issues are addressed using femtosecond (fs) nonlinear optical techniques.

The experiments were performed using visible ultrashort pulses derived from the signal beam of a 250 kHz regenerative amplifier-pumped optical parametric amplifier. These pulses were compressed to less than 60 fs and frequency doubled in β-barium borate (BBO) to obtain a source of continuously tunable ultraviolet pulses for pump-probe measurements. Pulses with center wavelengths varying from 250 nm to 375 nm can be readily obtained through angle tuning of the BBO crystal. Figure 1 illustrates the basic concept of the experimental technique. The ultraviolet pulses are split in two. One pulse, the pump

In *Photodetectors: Materials and Devices V*, Gail J. Brown, Manijeh Razeghi, Editors, Proceedings of SPIE Vol. 3948 (2000) • 0277-786X/00/$15.00

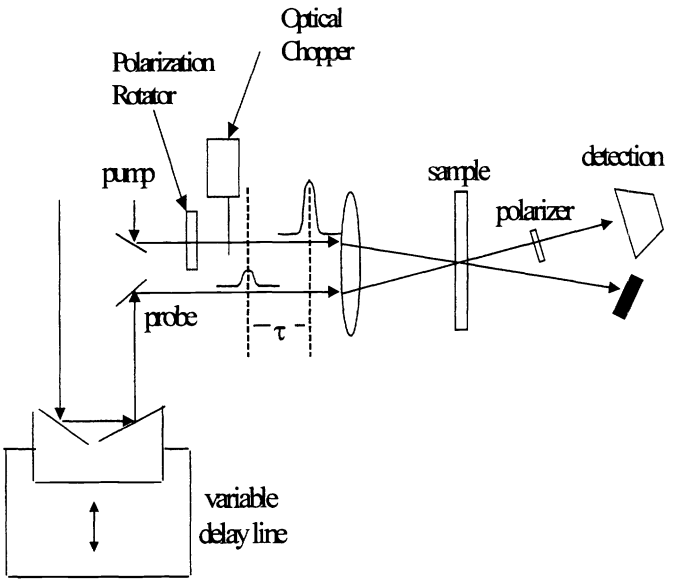

Figure 1 Schematic of a pump-probe experiment.

pulse, is used to create excitations (excitons, electron-hole pairs) in the sample. These excitations change the dielectric function of this material. The intensity of the other pulse, the probe pulse, is weak enough that it does not perturb the optical properties. What one detects, therefore, is the change in the probe-monitored optical properties of the sample associated with the pump-induced perturbation of the dielectric function. Since the relative change in the probe intensity is quite small, the pump intensity is modulated with an optical chopper, and the resultant modulation of the probe is detected at the chopping frequency using lock-in techniques. The pump and probe are cross linear polarized to enhance the rejection of scattered pump light. Performing this detection procedure as a function of a precisely controlled mechanical time delay enables one to study the dynamics of the pump-induced excitations with femtosecond resolution. Such resolution cannot be attained using conventional electronic techniques, which are limited to the picosecond (ps) regime.

In this paper we shall demonstrate the use of three embodiments of the pump-probe technique in the study of carrier dynamics in wide bandgap semiconductors relevant to the improvement of visible-blind and solar-blind detectors. Time-resolved reflectivity techniques have been used to compare carrier recombination dynamics in GaN grown by double lateral epitaxial overgrowth (DLEO) and GaN grown on sapphire without benefit of this technique. The electron velocity-field characteristic and saturation velocity in GaN have been obtained from time-resolved studies of electroabsorption in GaN p-i-n diodes. Time-resolved transmission measurements have been used to monitor ultrafast carrier relaxation phenomena in a thin AlGaN layer with bandgap in the solar blind region of the spectrum.

2. TIME-RESOLVED REFLECTIVITY STUDIES OF DOUBLE LEO AND NON-LEO GAN

It has been demonstrated that growth of GaN on sapphire by lateral epitaxial overgrowth[1-6] greatly reduces the threading dislocation density in this material. A device lifetime of more than 10000 h at room temperature has been reported for cw operation of InGaN multiple quantum well laser diodes employing LEO GaN grown by metalorganic chemical vapor deposition (MOCVD)[1], and a significant decrease of p-n junction reverse leakage current in LEO materials has also been observed[4]. These results suggest that growth of III-nitride ultraviolet detectors on LEO GaN/sapphire substrates may be an important step in the development of high quality devices. Nevertheless, little is known about the relationship between threading dislocation density and the room temperature carrier lifetime of resonantly created excitations with low excess energy crucial to an understanding of device performance.

We have addressed this problem by performing a comparison study of the carrier lifetimes in non-LEO and DLEO GaN grown on (0001) sapphire. The samples for this study were grown at the Center for Quantum Devices at Northwestern University. The non-LEO sample was a 2 μm film expected to have a large threading dislocation density. The structure of the DLEO sample is shown in figure 2. A 2 μm GaN template was grown on the sapphire substrate. The dielectric pattern deposited on this template consisted of 7.5μm-wide SiO_2 stripes separated by 4 μm openings. The GaN grows from the openings on either side of the stripes laterally over these stripes until coalescence occurs, as seen from the cross-sectional scanning electron microscope (SEM) image. The thickness of this first LEO layer is 2.2 μm. While the threading dislocation density is greatly reduced in the LEO material atop the stripes, dislocations still propagate vertically from the window regions. Therefore a second dielectric pattern is deposited in which the stripes are positioned above the openings in the first one, such that these stripes prevent the dislocations from continuing into the next LEO layer. This second layer is 3.2 μm thick and the SEM image indicates that it is also coalesced. The use of this DLEO structure ensures that the double coalesced material is nearly dislocation free over large areas, an important consideration for our measurements, for which the laser spot

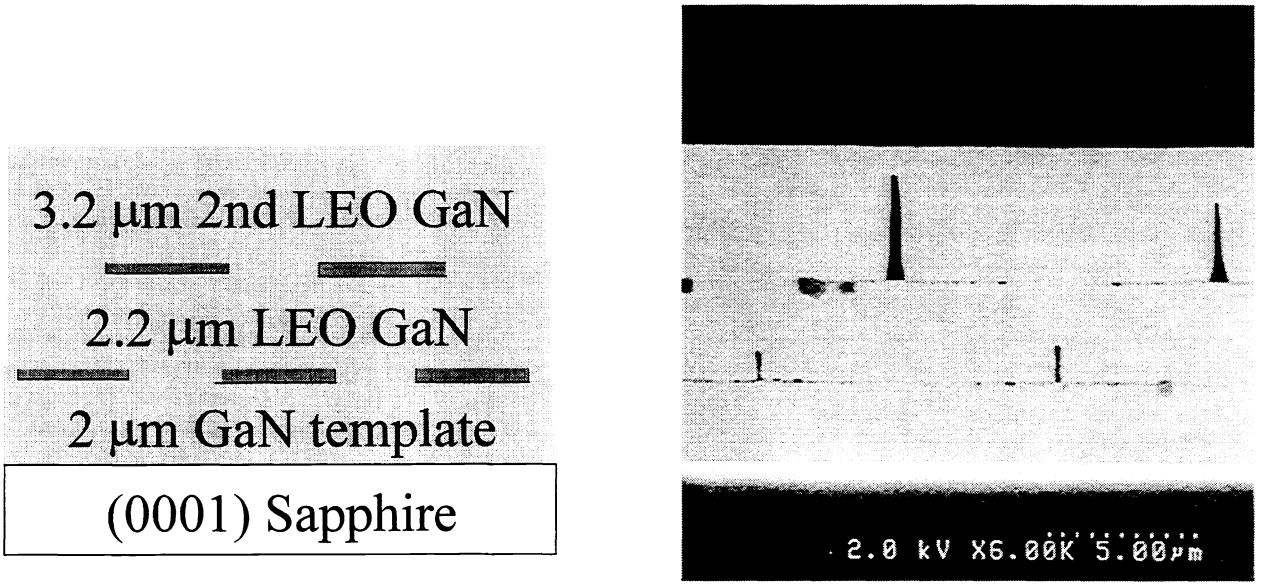

Figure 2 Schematic (left) and cross-sectional SEM image (right) of the double coalesced LEO grown-GaN on sapphire used in the time-resolved reflectivity experiment.

size is ~ 100 μm in diameter (i.e., much larger than the width of the stripes in the dielectric pattern). However, since the thickness of the samples is much greater than the 1000 Å absorption length for near bandgap photons, it is necessary to perform time-resolved reflectivity measurements.

For excitation of free carriers using photon energies near the bandgap of GaN, the change in the probe reflectivity ΔR is essentially proportional to the change in the real part of the dielectric function $\Delta\varepsilon_1$, which may be obtained from the spectral dependence of the change in the imaginary part of the dielectric function $\Delta\varepsilon_2$ by means of the Kramers-Kronig relation

$$\Delta R \propto \Delta\varepsilon_1(\omega) = \frac{2}{\pi}\int_0^\infty \frac{\omega'\Delta\varepsilon_2(\omega')d\omega'}{\omega'^2-\omega^2}, \tag{1}$$

where

$$\Delta\varepsilon_2(\omega) \sim -\varepsilon_2(\omega)\{f_h(E_h(\omega)) + f_e(E_e(\omega))\} \tag{2}$$

is a measure of the photoinduced bleaching associated with the absorption saturation of band-to-band transitions, and $f_e(E_e)$ and $f_h(E_h)$ are the electron and hole distribution functions at electron and hole excess energies E_e and E_h, respectively[7]. If the excess energies of the carriers is small, the parabolic band approximation may be invoked, and

$$E_{e,h} = \frac{m_r}{m_{e,h}}(\hbar\omega - E_g), \tag{3}$$

where $m_{e(h)}$ is the electron (hole) effective mass, $\hbar\omega$ is the photon energy, E_g is the bandgap energy, and m_r is the reduced effective mass, defined by the relation $m_r^{-1}=m_e^{-1}+m_h^{-1}$. For GaN the electron effective mass ($0.2m_o$) is much less than the hole effective mass ($\sim 2m_o$)[8]. Since equation 3 indicates that the ratio of the electron and hole excess energies is inversely proportional to the ratio of their effective masses, it follows that the electrons receive almost all of the excess energy from the excitation pulse. Moreover, in the parabolic band approximation the density of states is proportional to $m^{3/2}$, implying that the density of states near $\mathbf{k}=0$ in the conduction band is much smaller than that in the valence band. Therefore, for a given density

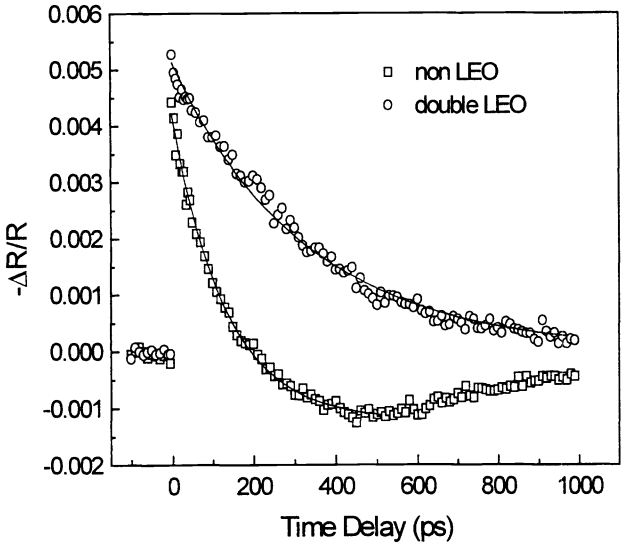

Figure 3 Comparison of time-resolved reflectivity data for non-LEO- and double LEO-grown GaN. The fits to the data are described in the text.

of electron-hole pairs, the contribution of the electron distribution to the photoinduced bleaching is much larger than that of the hole distribution, in accordance with equation 2. These observations suggest that our time-resolved photo-induced reflectivity measurements primarily probe the electron dynamics.

Figure 3 shows the relative change in probe reflectivity $-\Delta R/R$ as a function of time delay between the pump and probe pulses for the non-LEO and DLEO samples. The photon energy of the frequency degenerate pump and probe pulses was centered at ~ 3.4 eV, thus ensuring the creation of carriers with very little excess energy. At negative time delays, for which the probe precedes the pump, no signal is observed. When the pump and probe pulses are temporally overlapped at $t=0^+$, a sharp, pulse width-limited negative ΔR occurs. For the non-LEO sample, this quantity decays much more rapidly than it does for the DLEO material, reaching a positive value not observed for its DLEO counterpart. While the data in figure 3 was obtained for a carrier density of $\sim 2\times10^{18}$ cm^{-3}, the shapes of the decay curves were not significantly affected by changes in the pump intensity.

For excitation and probing at a photon energy corresponding to the bandgap, equation 1 suggests that $\Delta\varepsilon_1$ should possess the same sign as $\Delta\varepsilon_2$. The creation of carriers at the band edge by the pump causes a bleaching of the probe absorption and therefore a negative $\Delta\varepsilon_2$, as seen from equation 2, and a negative $\Delta\varepsilon_1$ (ΔR) at $t=0^+$. In this case the ΔR decays represent the removal of electron-hole pairs from the bottom of the bands by either band-to-band recombination or trapping at deep levels and subsequent recombination. The positive ΔR observed at later times in the non-LEO data implies that $\Delta\varepsilon_2$ also becomes positive, perhaps signifying an increase in absorption at photon energies higher than that of the probe due to bandgap shrinkage associated with the heating of the sample. This behavior suggests that the dominant ΔR decay mechanism in the non-LEO sample is ultrafast nonradiative recombination and heat generation, with the positive component's subsequent return to equilibrium on a nanosecond time scale representative of heat diffusion out of the optically probed region. A single exponential fit that incorporates this heating yields a decay time of 130 ps, in excellent agreement with the data. The fact that there is no positive component to the ΔR decay in the DLEO sample implies that ultrafast nonradiative recombination is greatly reduced and that the carriers are removed from the bands primarily by band-to-band radiative recombination. A single exponential decay with a time constant of 330 ps provides an excellent fit to the data.

While these results support observations that a stronger photoluminescence (PL) signal occurs in LEO materials than in non-LEO samples, they also indicate that the reduction in threading dislocations achieved through LEO growth leads to an increase in the carrier lifetime due to suppression of ultrafast nonradiative recombination mechanisms associated with the highly dislocated non-LEO material. Time-resolved photoluminescence (TRPL) measurements capable of discriminating between the window and high quality materials in an LEO sample[9] yielded a dominant decay time of 130 ps for both cases when excitation pulses of 4.64 eV photon energy were employed. The fact that the PL from the LEO material was more intense than that from the window material in conjunction with the TRPL result was interpreted to mean that under these excitation conditions the threading dislocations simply reduce the net volume of light-emitting area without affecting the luminescence lifetime. Experiments performed using near bandgap resonant excitation[10,11] yield carrier lifetimes more consistent with our data. Low temperature ΔR studies of resonantly excited exciton dynamics in LEO metalorganic vapor phase epitaxy (MOVPE) material[10] and TRPL studies of thick (63 μm) hydride vapor phase epitaxy (HVPE) material[11] yield free exciton lifetimes of 375 ps at 60 K and 295 ps at 4 K, respectively. These results are in good agreement with theoretical predictions of the radiative lifetime[10]. At room temperature the lifetime is expected to be longer due to a thermally induced

increase in the center of mass kinetic energy of the excitons[11]. The fact that this phenomenon does not occur in our DLEO sample is attributed to the diffusion of Si impurities from the dielectric stripes into the DLEO material during the high temperature growth process. It is therefore expected that the room temperature lifetime will increase for thicker DLEO layers, in which the diffusion of silicon should not be as important. This behavior has been observed for thicker (~5 μm) LEO material[12].

3. TIME-RESOLVED ELECTROABSORPTION STUDIES OF ELECTRON TRANSPORT IN GAN

Theoretical calculations[13-16] of the electron velocity-field characteristic in GaN predict a peak steady-state velocity of 2-3×10^7 cm/sec, implying that this material may be an important candidate for high frequency devices. Although ultrawide-bandwidth AlGaN/GaN heterostructure field effect transistors[17-20] and very high-speed[21], transit-time-limited GaN metal-semiconductor-metal (MSM)[22,23] and *p-i-n*[24] ultraviolet photodetectors have been demonstrated, no direct measurements of carrier velocities in III-N materials have been reported. Such studies will help to determine the ultimate speed of electronic devices and provide reliable high field transport data for the design of solar blind detectors based on avalanche photodiodes. In this paper we present the first measurement of the electron velocity at high electric fields in GaN. An optically-detected time-of-flight technique[25,26] with femtosecond resolution that monitors the change in the electroabsorption due to charge transport in a GaN *p-i-n* diode has been used to determine the electron velocity-field characteristic at room temperature.

The sample used in this study was fabricated and electrically characterized at the University of Texas at Austin and the U.S. Military Academy at West Point. The nominal thicknesses of the *p*-layer, intrinsic (ν-type) region, and *n*-layer are 0.2 μm, 0.5 μm, and 3.4 μm, respectively. The doping levels of the *n*-GaN and ν-GaN are ~ 5×10^{18} cm^{-3} and ~2×10^{16} cm^{-3}, respectively, as confirmed by Hall effect measurements on test samples, and capacitance-voltage (CV) measurements performed on the fabricated diodes. The *p*-type doping level was estimated from Hall measurements of single epitaxial layers to be ~1-2 $\times10^{17}$ cm^{-3}. The diameter of the fabricated mesa isolated diode is 250 μm. A ring top contact is used to allow for penetration of the incident light pulses.

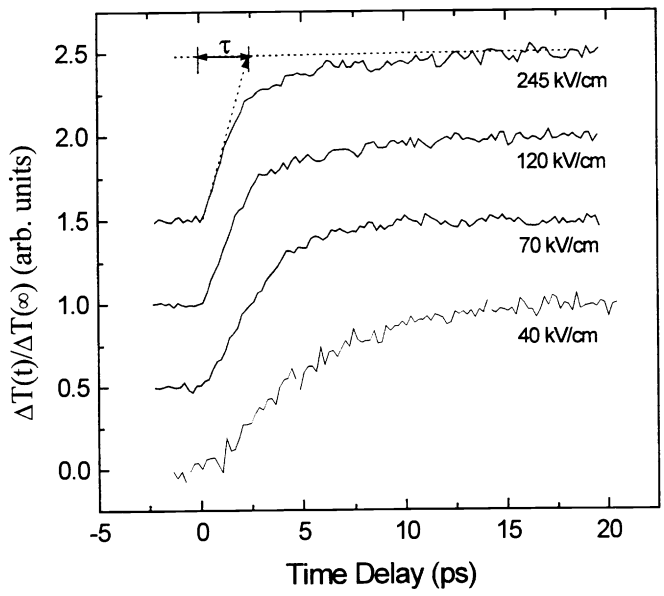

Figure 4 Normalized photoinduced bleaching of the p-i-n diode electroabsorption as a function of time delay for four electric fields. The method of obtaining the transit time from the initial slope and the plateau of the transient is illustrated for the 245 kV/cm curve.

The pump and probe pulses were incident on the *p*-layer of the sample. The spectrum of the pump pulse was centered at 3.41 eV, a photon energy corresponding to the peak photocurrent of the device. This choice of photon energy, at which the absorption length is only ~0.1μm, ensured that almost all of the photogenerated carriers contributing to the photocurrent were generated near the interface of the *p*-type layer and the *i*-region[27]. The diode was biased using 200 ns voltage pulses synchronized with the optical pulses. The change in transmission ΔT of the probe was monitored at a sub-bandgap photon energy chosen to maximize the sensitivity of this quantity to a change in the broadening of the absorption edge under applied electric field (Franz-Keldysh effect). Pump-generated electrons and holes moving under the applied plus built-in electric field E are swept toward the *n*- and *p*-layers, respectively. As the carriers drift apart, a space-charge field of opposite sign creates a potential difference that grows in time until transport is completed. The pump-induced charge density is kept low enough that this screening field ΔE is much smaller than E. The space-charge field causes a reduction in the broadening of the absorption edge and concomitant induced bleaching of the relative probe transmission given in the thick sample limit by[26]

$$\frac{\Delta T(t)}{T} = -\frac{d\alpha_p}{dE}\int_0^d \Delta E(x,t)dx = \frac{d\alpha_p}{dE}\delta V(t), \tag{4}$$

where α_p is the probe absorption coefficient, d is the length of the region over which the field is applied (i.e., the depletion width obtained from CV measurements), $\delta V(t)$ is the change in voltage across the sample due to photocarrier transport, and reflectivity corrections have been neglected. The change in voltage occurs because the response time of the external bias circuit is too slow to maintain a constant potential difference during the transit time of the carriers. This situation is in direct contrast to photocurrent detection experiments, in which the voltage must recover during the transit time such that the photocurrents flowing in the external bias circuit transfer a photocharge $Q(t)$ to the electrodes that exactly cancels $\delta V(t)$.

Figure 4 shows the normalized bleaching $\Delta T(t)/\Delta T(\infty)$ as a function of time delay for four electric fields. The normalization factor $\Delta T(\infty)$ refers to the change in transmission after all the carriers have traversed the sample. All of these curves are characterized by a quasi-linear increase in this quantity that begins at t=0 and eventually reaches a plateau at $\Delta T(t)/\Delta T(\infty)$ =1. The fact that the sharp rise in transmission normally observed at t=0 in pump-probe experiments is not present in this case indicates that the pump-generated carrier density is small enough to avoid the creation of any change in the probe transmission in the absence of field-induced transport. As the electrons and holes drift apart in the electric field, the normalized bleaching rises in accordance with equation 4, with the plateau occurring when the carriers cease to move apart. In analogy to the treatment in reference 25, the normalized change in transmission can be expressed as

$$\frac{\Delta T(t)}{\Delta T(\infty)} = \frac{\int v_e dt - \int v_h dt \exp(-\alpha d) + \alpha^{-1}\{1 - \exp(-\alpha \int v_h dt) + \exp(-\alpha d)[1 - \exp(\alpha \int v_e dt)]\}}{d[1 - \exp(-\alpha d)]}, \tag{5}$$

where α is the pump absorption coefficient, v_e and v_h are the electron and hole velocities, respectively, t is the time delay between the pump and probe pulses, and diffusion has been neglected. The slope of this function near t=0 is given by

$$\frac{\partial}{\partial t}\frac{\Delta T(t)}{\Delta T(\infty)} \equiv \frac{1}{\tau} \cong \frac{v_e + v_h}{d}, \tag{6}$$

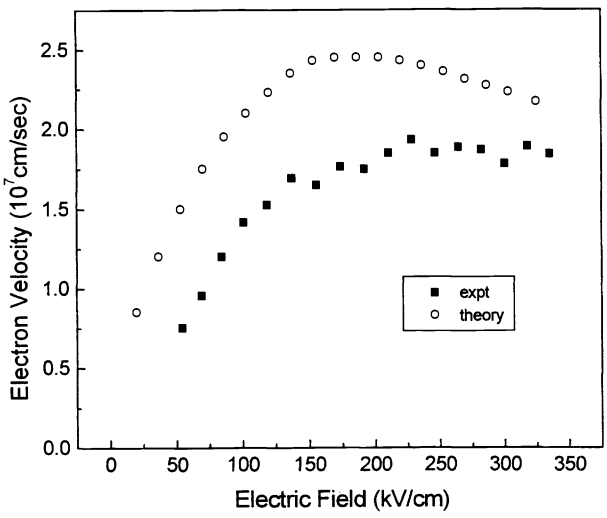

Figure 5 Steady-state electron velocity as a function of electric field. Squares: experiment; Circles: theoretical calculation using a full zone band structure (from ref. 13).

where v_e and v_h are assumed to be constant and τ is defined as the transit time across the sample, as depicted in figure 4. Since the carriers are generated at the interface of the p- and i-layers, the electrons drift much further than the holes, and the majority of the signal is due to electron transport. It is therefore a reasonable approximation to take τ as the electron transit time. The fact that the slope of the normalized bleaching curves increases with increasing field indicates that the electron transit time decreases and velocity increases, as expected. One may also notice, however, that the slope changes more with increasing electric field at low fields than it does at high fields. This phenomenon implies that the electron transit time and velocity become 'saturated' – i.e., relatively independent of electric field – at high fields.

The experimentally determined electron velocity shown in figure 5 was obtained using equation 6. Although theoretical calculations of the hole velocity[28] suggest that v_h is less than $0.15v_e$ over the entire range of electric fields employed in our experiments, the calculated v_h was included in equation 6 to achieve a more accurate estimate of the electron velocity. At the lowest fields for which

measurements were performed, v_e possesses a weak, quasi-linear dependence on E. Extrapolation of the results to zero field does not provide a realistic estimate of the low-field mobility, however, as ensemble Monte Carlo (EMC) calculations employing multi-valley analytic band structures[14-16] predict a steeper linear rise in the velocity-field characteristic only at fields (0-20kV) much less than the smallest field used in our experiments. In the intermediate field regime (50-100kV) corresponding to our low field measurements, electrons attain enough excess energy to emit polar optical phonons, causing the theoretical velocity-field characteristic to transition to a low slope region[14] more representative of our data.

In the high field regime the electron velocity gradually becomes independent of electric field, reaching a peak of 1.9 $\times 10^7$ cm/sec at ~ 225 kV/cm corresponding to a transit time of ~2.5 ps. At fields greater than 250 kV/cm, the apparent slight decline in the electron velocity obtained from equation (6) for saturated transit time is indicative of a monotonically increasing hole velocity[28] in this electric field range. The steady-state velocity-field characteristic derived from an EMC calculation including a full Brillouin zone band structure[13] is shown in figure 5 for comparison with the measurements. The theoretical results are in qualitative agreement with the data. The fact that the peak velocity obtained from experiment is lower and shifted to higher field than its theoretical counterpart suggests that the high defect density of the device, not accounted for by theory, may play an important role in determining the velocity-field characteristic. It has also been shown[15] that decreasing the separation of the two lowest conduction bands at the Γ point from ~2 eV to the 0.34 eV value obtained from ballistic electron emission microscopy[29] results in a reduction in peak velocity and a velocity-field characteristic in closer agreement with our data.

As a further check on the validity of the experimental results, equation 5 was used to fit the $\Delta T(t)/\Delta T(\infty)$ curves for the electric fields corresponding to each of the data points in figure 5. The electron velocity-field characteristic obtained from these fits falls directly on top of the data shown in this figure. The fact that a single steady-state electron velocity approximation could be used to fit the temporal evolution of each normalized bleaching curve justifies the assumption that for our experimental conditions the majority of the transport across the 0.5 μm *i*-region is not strongly influenced by velocity overshoot effects. This result is supported by theoretical calculations[16] that predict that the velocity overshoot is completed within ~ 200 fs, during which time the electrons may still be moving in the nonuniform field near the interface of the *p*- and *i*-layers.

4. TIME-RESOLVED TRANSMISSION STUDIES OF SOLAR BLIND ALGAN

The solar blind region of the spectrum (< 280 nm) is attractive for ultraviolet detector applications because it offers the possibility of nearly background-free, uncooled detection. While prototype photoconductive[30-32] and photovoltaic[33,34] detectors have been fabricated, little is known about the carrier dynamics in the solar blind materials comprising these devices. We have performed time-resolved transmission measurements on solar blind AlGaN provided by the Center for Quantum Devices at Northwestern University. The sample used in this study is a 190 nm $Al_xGa_{1-x}N$ layer with x=38.6%, as determined by X-ray diffraction, grown on an AlN buffer layer deposited on (0001) sapphire. In these experiments the change in transmission ΔT of the probe pulse due to electron-hole pairs excited by the pump is monitored as a function of time delay between the pump and probe. Since the AlGaN layer is about two absorption lengths thick, it is reasonable to assume that ΔT is approximately proportional to $\Delta\varepsilon_2$, where $\Delta\varepsilon_2$ is given by equation 2 for pump-induced bleaching of band-to-band transitions. Momentum (**k**) conservation in this case dictates that for the frequency degenerate pulses employed in the experiments the probe monitors the same states optically coupled by the pump. Therefore the ΔT decay provides information primarily about the rate at which electrons (per our discussion in section 2) are removed from their initial states by scattering, trapping, or recombination. Moreover, by performing these measurements as a function of photon energy and pump intensity, information about the various relaxation mechanisms can be obtained.

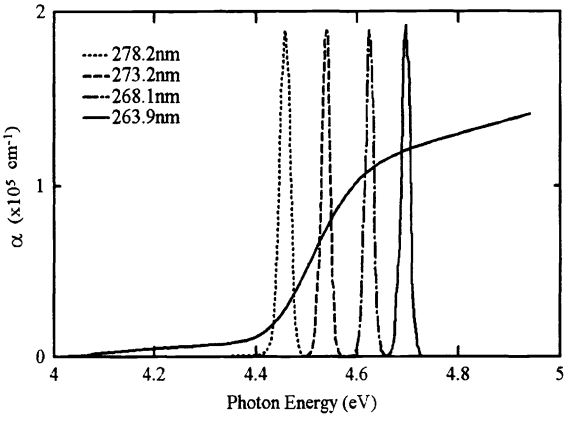

Figure 6 Absorption spectrum of a 190 nm $Al_xGa_{1-x}N$ layer with x=38.6%. Superimposed are the laser pulse spectra corresponding to the four center wavelengths at which time-resolved transmission measurements were performed.

Figure 6 shows the absorption coefficient α of the AlGaN layer estimated from transmission measurements. A standard linear fit of α^2 versus $(\hbar\omega - E_g)$ yields E_g= 4.47 eV.

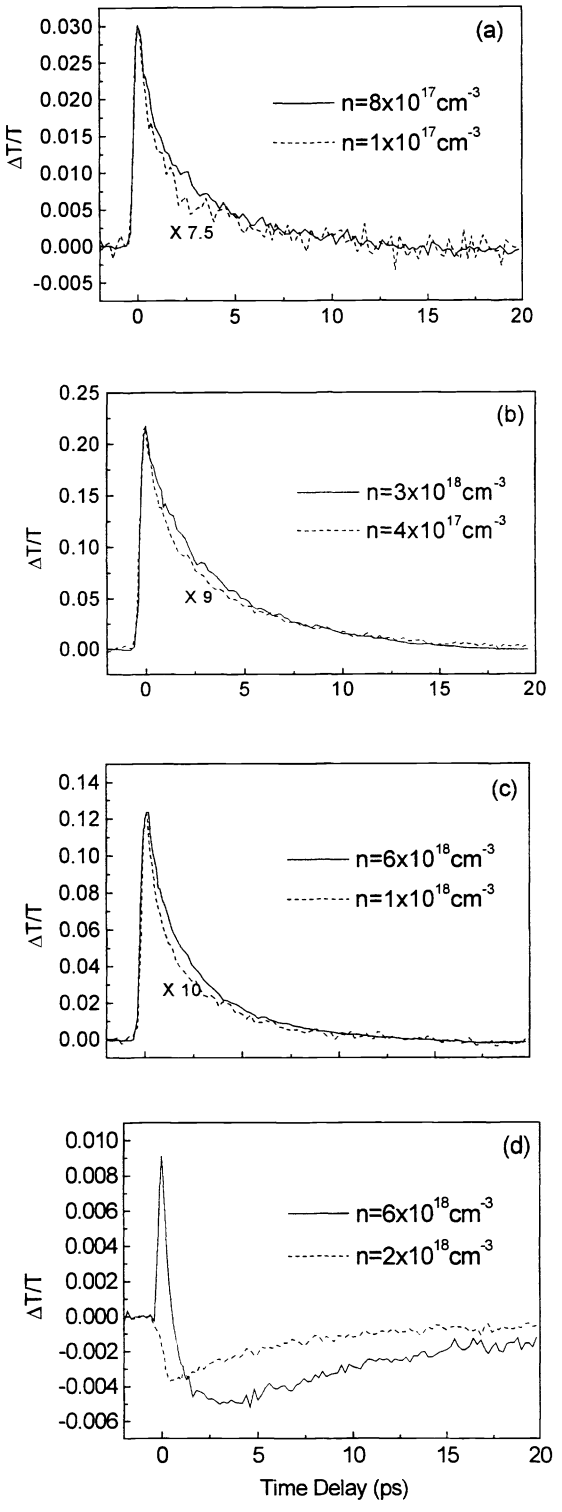

Figure 7 Normalized change in probe transmission as a function of time delay for center wavelength of (a) 278.2 nm; (b) 273.2 nm; (c) 268.1 nm; (d) 263.9 nm.

The rise in the fundamental absorption possesses a width of ~100 meV. Superimposed on the absorption spectrum in figure 6 are the laser pulse spectra corresponding to four center wavelengths at which time-resolved transmission measurements representative of the carrier dynamics in this material were performed.

Figure 7 shows the results of these experiments. In all cases the higher intensity excitation data exhibits a pulse-width-limited rise in ΔT at $t=0^+$ due to the pump-induced bleaching described above, followed by an ultrafast decay. We shall define the decay time τ as the time at which ΔT decays to half its maximum value. For the 278.2 nm experiment (fig. 7a) the photon energy (4.457 eV) is less than the bandgap, and the presence of a significant bleaching signal implies that shallow traps exist below the band edge(s). The observation that the decay time decreases from 1.1 ps to 0.8 ps when the excitation density is reduced by a factor of 8 suggests that the bleaching decays by trapping to deeper levels, and that the partial saturation of these deep traps causes τ to increase with increasing intensity. Similar behavior is found in the 273.2 nm excitation data (fig. 7b), for which τ decreases from 2 ps to 1.3 ps when the carrier density is lowered by a factor of 8, but remains the same as the pump intensity is lowered by another order of magnitude. The photon energy (4.539 eV) in this case is sufficient to create cold electron-hole pairs in the conduction and valence bands, and the stronger bleaching observed is indicative of both the larger carrier density and the rise in ε_2, which at this wavelength is approximately proportional to α in fig. 6. Since much longer carrier relaxation times are found for excitation of cold electron-hole pairs in high quality GaN[12], the decays in fig. 7b are attributed to electron relaxation from extended states into shallow traps. Comparison of the data in figs. 7a and 7b indicates that this process appears to take longer than trapping from shallow to deep levels. The saturation behavior of the bleaching decays in these two figures suggests that the densities of shallow and deep traps are in the mid- to upper $10^{17}cm^{-3}$ range.

For shorter wavelength excitation (figs. 7c and 7d), hot electrons with excess energy much larger than the bandwidth of states optically coupled by the probe are created. In these cases the bleaching decays provide information about scattering from the optically coupled states. For 268.1 nm excitation (fig. 7c) the peak normalized bleaching signal drops by a factor of 10 and τ decreases from 1.2 ps to 0.9 ps when the carrier density is lowered from 6 to $1\times10^{18}cm^{-3}$. This behavior suggests that a very fast scattering process is screened at the higher density. In polar semiconductors like the III-nitrides, the dominant electron energy loss mechanism for low excitation densities is electron-longitudinal optical (LO) phonon scattering, which is expected to occur on a time scale less than the ~200 fs temporal resolution of our experiment[35]. At intermediate excitation densities the electron-LO phonon interaction is partially screened, and electron-transverse optical (TO) phonon scattering and electron-

hole scattering, through which the hot electrons lose energy to the much colder holes, also become important. Since the decay time ascribed to this process in high quality LEO GaN is ~35 ps under similar excitation conditions[12], the 1.2 ps time constant in our AlGaN sample suggests that trapping still plays a role. Moreover, the fact that τ does not become much smaller as the carrier density is lowered implies that only part of the electron distribution has sufficient energy to emit LO phonons. At the photon energy employed in this experiment (4.625 eV) the electrons and holes share 155 meV of excess energy. While this excess energy level would lead to electron energy loss by LO phonon emission at low excitation density in GaN, it may not do so in our AlGaN sample. Due to the wider bandgap of AlGaN, the ratio m_e/m_h is expected to be larger than that observed in GaN, in which case the holes would receive a greater proportion of the excess energy. In addition, the LO phonon energy for AlGaN with 40% Al content is ~102 meV[36,37], higher than the 92 meV found in GaN. These two factors may combine to create the experimental situation in AlGaN at low excitation density proposed above.

This concept is supported by the 263.9 nm (4.7 eV) data in fig. 7d. In this case the peak normalized bleaching under intermediate excitation conditions is much weaker than in the previous data, and the 180 fs decay time is indicative of the temporal resolution of the experiment. The bleaching rapidly evolves into induced absorption, which decays on a longer (~10 ps) time scale. When the carrier density is reduced by a factor of 3, the bleaching component of ΔT disappears entirely, and the induced absorption reaches a peak at 0.4 ps that decays with a 4 ps time constant. The rapid decay of the weak bleaching into induced absorption for the higher carrier density data implies that most of the electrons have sufficient energy to relax via both the partially screened electron-LO phonon interaction and the other scattering mechanisms described above, and are trapped quickly into deep levels. While nonradiative recombination and concomitant ultrafast heat production would also lead to induced absorption (section 2), the decay of the $-\Delta T$ component of the signal is much faster than expected for heat diffusion out of the optical spot size. The induced absorption is therefore attributed to the re-excitation of electrons from the deep levels into the conduction band, in analogy to results obtained from similar measurements on low-temperature-grown (LT) GaAs[38]. Viewed in this way, the lack of a bleaching signal for the lower intensity data suggests that at a carrier density of $2\times10^{18}cm^{-3}$ the screening of the electron-LO phonon interaction is reduced enough that the relaxation time is beyond our temporal resolution, a phenomenon previously observed in GaN at about the same carrier density[12]. Moreover, the rise in the induced absorption may be interpreted as the deep level trapping time, and its decay as the emptying of the traps by recombination. It appears that this trapping time becomes faster when the electrons possess larger excess energy, a behavior also found in LT-GaAs.

The parallels between our AlGaN and LT-GaAs may be partially explained by the fact that our AlGaN was grown on an AlN buffer layer. Because the melting point of the AlN is extremely high, the deposition of the AlN on sapphire behaves like a low temperature growth, and the AlN possesses significant surface roughness. Subsequent growth of a thin AlGaN layer on top of the AlN therefore produces the high defect density material characterized in this paper. This interpretation is consistent with the observations of other researchers that at high Al content the buffer layer defects are replicated into an AlGaN layer[39], and that the PL spectrum excited from an AlGaN/sapphire interface shows an additional narrow peak below the band edge attributed to interfacial defects[40]. Thus, time-resolved transmission measurements can be used to evaluate the quality of both thin AlGaN films and their AlN buffer layers.

5. CONCLUSION

In this paper we have demonstrated that femtosecond nonlinear optical techniques can be employed both in the creation of a continuously tunable source of ultraviolet pulses and in the study of carrier dynamics and transport in ultraviolet detector materials using this source. Visible femtosecond pulses derived from the signal beam of a 250 kHz regenerative amplifier-pumped optical parametric amplifier were frequency doubled to obtain pulses tunable from 250 nm to 375 nm. Time-resolved reflectivity experiments indicate that the room-temperature carrier lifetime in GaN grown by double lateral epitaxial overgrowth (330 ps) is about 3 times longer than that of GaN grown on sapphire without benefit of this technique (130 ps). The electron velocity-field characteristic and saturation velocity in GaN have been obtained from time-resolved studies of electroabsorption in a GaN p-i-n diode. The peak steady-state velocity of 1.9×10^7 cm/s in this device occurs at 225 kV/cm. Time-resolved transmission measurements have been used to monitor ultrafast carrier relaxation phenomena in a thin AlGaN layer with bandgap in the solar blind region of the spectrum. Excitation intensity and wavelength dependent studies of the photoinduced bleaching decays suggest that they are primarily governed by trapping in a high density of sub-bandgap defect levels.

ACKNOWLEDGEMENTS

The researchers at the Center for Quantum Devices would like to acknowledge M. Yoder, C. Wood and Y.S. Park from ONR, and E. Martinez from DARPA. The work at CQD was supported by ONR/DARPA through grant No. N00014-99-1-0016. The work at the University of Texas at Austin was supported by the Army Research Office under DAAH04-93-G-0317, and by DARPA under contract MDA972-95-3-000.

REFERENCES

1. S. Nakamura, M. Senoh, S. Nagahama, N. Iwasa, T. Yamada, T. Matsushita, H. Kiyoku, Y. Sugimoto, T. Kozaki, H. Umemoto, M. Sano, and K. Chocho, "InGaN/GaN/AlGaN-based laser diodes with modulation-doped strained-layer superlattices grown on an epitaxially laterally overgrown GaN substrate", *Appl. Phys. Lett.* **72**, pp. 211-213, 1998.
2. D. Kapolnek, S. Keller, R. Vetury, R.D. Underwood, P. Kozodoy, S.P. DenBaars, and U.K. Mishra, "Anisotropic epitaxial lateral growth in GaN selective area epitaxy", *Appl. Phys. Lett.* **71**, pp. 1204-1206, 1997.
3. O.-H. Nam, M.D. Bremser, T.S. Zheleva, and R.F. Davis, "Lateral epitaxy of low defect density GaN layers via organometallic vapor phase epitaxy", *Appl. Phys. Lett.* **71**, pp. 2638-2640, 1997.
4. C. Sasaoka, H. Sunakawa, A. Kimura, M. Nido, A. Usui, and A. Sakai, "High-quality InGaN MQW on low-dislocation-density GaN substrate grown by hydride vapor-phase epitaxy", *J. Cryst. Growth* **189/190**, pp. 61-66, 1998; P. Kozodoy, J.P. Ibbetson, H. Marchand, P.T. Fini, S. Keller, J.S. Speck, S.P. DenBaars, and U.K. Mishra, "Electrical characterization of GaN p-n junctions with and without threading dislocations", *Appl. Phys. Lett.* **73**, pp. 975-977, 1998.
5. J. Park, P.A. Grudowski, C.J. Eiting, and R.D. Dupuis, "Selective-area and lateral epitaxial overgrowth of III-N materials by metal organic chemical vapor deposition", *Appl. Phys. Lett.* **73**, pp. 333-335, 1998.
6. P. Kung, D. Walker, M. Hamilton, J. Diaz, and M. Razeghi, "Lateral epitaxial overgrowth of GaN films on sapphire and silicon substrates", *Appl. Phys. Lett.* **74**, pp. 570-572, 1999.
7. D.H. Auston, S. McAfee, C.V. Shank, E.P. Ippen, and O. Teschke, "Picosecond spectroscopy of semiconductors", *Solid State Elec.***21**, pp. 147-150, 1978.
8. J.S. Im, A. Moritz, F. Steuber, V. Härle, F. Scholz, and A. Hangleiter, "Radiative carrier lifetime, momentum matrix element, and hole effective mass in GaN", *Appl. Phys. Lett.* **70**, pp. 631-633, 1997.
9. S.F. Chichibu, H. Marchand, M.S. Minsky, S. Keller, P.T. Fini, J.P. Ibbetson, S.B. Fleischer, J.S. Speck, J.E. Bowers, E. Hu, U.K. Mishra, S.P. DenBaars, T. Deguchi, T. Sota, and S. Nakamura, "Emission mechanisms of bulk GaN and InGaN quantum wells prepared by lateral epitaxial overgrowth", *Appl. Phys. Lett.* **74**, pp. 1460-1462, 1999.
10. S. Hess, F. Walraet, R.A. Taylor, J.F. Ryan, B. Beaumont, and P. Gibart, "Dynamics of resonantly excited excitons in GaN", *Phys. Rev. B* **58**, pp. R15973-R15976, 1998.
11. G.E. Bunea, W.D. Herzog, M.S. Ünlü, B.B. Goldberg, and R.J. Molnar, "Time-resolved photoluminescence studies of free and donor-bound exciton in GaN grown by hydride vapor phase epitaxy", *Appl. Phys. Lett.* **75**, pp. 838-840, 1999.
12. M. Wraback, H. Shen, C.J. Eiting, J.C. Carrano, and R.D. Dupuis, "Picosecond photoinduced reflectivity studies of GaN prepared by lateral epitaxial overgrowth", to appear in *MRS Internet J. Nitride Semicond. Res.*, 1999.
13. J. Kolnik, I.H. Oğuzman, K.F. Brennan, R. Wang, P.P. Ruden, and Y. Wang, "Electronic transport studies of bulk zinc-blende and wurtzite phases of GaN based on an ensemble Monte Carlo calculation including a full zone band structure", *J. Appl. Phys.* **78**, pp. 1033-1038, 1995.
14. U.V. Bhapkar and M.S. Shur, "Monte Carlo calculation of velocity-field characteristics of wurtzite GaN", *J. Appl. Phys.* **82**, pp. 1649-1655, 1997.
15. J.D. Albrecht, R.P. Wang, P.P. Ruden, M. Farahmand, and K.F. Brennan, "Electron transport characteristics of GaN for high temperature device modeling", *J. Appl. Phys.* **83**, pp. 4777-4781, 1998.
16. B.E. Foutz, S.K. O'Leary, M.S. Shur, and L.F. Eastman, "Transient electron transport in wurtzite GaN, InN, and AlN", *J. Appl. Phys.* **85**, pp. 7727-7734, 1999.
17. M.A. Khan, Q. Chen, M.S. Shur, B.T. Dermott, J.A. Higgins, J. Burm, W.J. Schaff, and L.F. Eastman, "CW operation of short-channel GaN/AlGaN doped channel heterostructure field effect transistors at 10 GHz and 15 GHz", *IEEE Electron Device Lett.* **17**, pp. 584-585, 1996.
18. J. Burm, K. Chu, W.J. Schaff, L.F. Eastman, M.A. Khan, Q. Chen, J.W. Yang, and M.S. Shur, "0.12 μm gate III-V nitride HFET's with high contact resistances", *IEEE Electron Device Lett.* **18**, pp. 141-143, 1997.

19. Y.-F. Wu, B.P. Keller, S. Keller, N.X. Nguyen, M. Le, C. Nguyen, T.J. Jenkins, L.T. Kehias, S.P. DenBaars, and U.K. Mishra, "Short channel AlGaN/GaN MODFET's with 50-GHz f_T and 1.7 W/mm output-power at 10 GHz", *IEEE Electron Device Lett.* **18**, pp. 438-440, 1997.
20. A.T. Ping, Q. Chen, J.W. Yang, M.A. Khan, and I. Adesida, "DC and microwave performance of high-current AlGaN/GaN heterostructure field effect transistors grown on p-type SiC substrates", *IEEE Electron Device Lett.* **19**, pp. 54-56, 1998.
21. J.C. Carrano, T. Li, C.J. Eiting, R.D. Dupuis, and J.C. Campbell, "Very high-speed ultraviolet photodetectors fabricated on GaN", *J. Electron. Mat.* **28**, pp. 325-333, 1999.
22. J.C. Carrano, T. Li, D.L. Brown, P.A. Grudowski, C.J. Eiting, R.D. Dupuis, and J.C. Campbell, "Very high-speed metal-semiconductor-metal ultraviolet photodetectors fabricated on GaN", *Appl. Phys. Lett.* **73**, pp. 2405-2407, 1998.
23. D. Walker, E. Monroy, P. Kung, M. Hamilton, F.J. Sanchez, J. Diaz, and M. Razeghi, "High speed, low noise metal-semiconductor-metal ultraviolet photodetectors based on GaN", *Appl. Phys. Lett.* **74**, pp. 762-764, 1999.
24. J.C. Carrano, T. Li, D.L. Brown, P.A. Grudowski, C.J. Eiting, R.D. Dupuis, and J.C. Campbell, "High-speed p-i-n ultraviolet photodetectors fabricated on GaN", Electron. Lett. **34**, pp. 1779-1781, 1998.
25. C.V. Shank, R.L. Fork, B.I. Greene, F.K. Reinhart, and R.A. Logan, "Picosecond nonequilibrium carrier transport in GaAs", *Appl. Phys. Lett.* **38**, pp. 104-105, 1981.
26. E.A. Schiff, R.I. Devlen, H.T. Grahn, J. Tauc, and S. Guha, "Picosecond electron drift mobility measurements in hydrogenated amorphous silicon", *Appl. Phys. Lett.* **54**, pp. 1911-1913, 1989.
27. T. Li, J.C. Carrano, J.C. Campbell, M. Schurman, and I. Ferguson, "Analysis of external quantum efficiencies of GaN homojunction p-i-n ultraviolet photodetectors", *IEEE J. Quantum Electron.* **35**, pp. 1203-1206, 1999.
28. I.H. Oğuzman, J. Kolnik, K.F. Brennan, R. Wang, T.-N. Fang, and P.P. Ruden, "Hole transport properties of bulk zinc-blende and wurtzite phases of GaN based on an ensemble Monte Carlo calculation including a full zone band structure", *J. Appl. Phys.* **80**, pp. 4429-4436, 1996.
29. E.G. Brazel, M.A. Chin, V. Narayanamurti, D. Kapolnek, E.J. Tarsa, and S.P. DenBaars, "Ballistic electron emission microscopy study of transport in GaN thin films", *Appl. Phys. Lett.* **70**, pp. 330-332, 1997.
30. B.W. Lim, Q.C. Chen, J.Y. Yang, and M.A. Khan, "High responsivity intrinsic photoconductors based on $Al_xGa_{1-x}N$", *Appl. Phys. Lett.* **68**, pp. 3761-3762, 1996.
31. D. Walker, X. Zhang, A. Saxler, P. Kung, J. Xu, and M. Razeghi, "$Al_xGa_{1-x}N$ ($0<x\leq1$) ultraviolet photodetectors grown on sapphire by metal-organic chemical-vapor deposition," *Appl. Phys. Lett.* **70**, pp. 949-951, 1997.
32. M. Misra, D. Korakakis, H.M. Ng, and T.D. Moustakas, "Photoconductive detectors based on partially ordered $Al_xGa_{1-x}N$ alloys grown by molecular beam epitaxy", *Appl. Phys. Lett.* **74**, pp. 2203-2205, 1999.
33. A. Osinsky, S. Gangopadhyay, B.W. Lim, M.Z. Anwar, M.A. Khan, D.V. Kuksenkov, and H. Temkin, "Schottky barrier photodetectors based on AlGaN", *Appl. Phys. Lett.* **72**, pp. 742-744, 1998.
34. D. Walker, V. Kumar, K. Mi, P. Sandvik, P. Kung, X.H. Zhang, and M. Razeghi, "Solar-blind AlGaN photodiodes with very low cutoff wavelength," *Appl. Phys. Lett.* **76**, pp. 403-405, 2000.
35. K.T. Tsen, D.K. Ferry, A. Botchkarev, B. Sverdlov, A. Salvador, and H. Morkoc, "Direct measurements of electron-longitudinal optical phonon scattering rates in wurtzite GaN", *Appl. Phys. Lett.* **71**, pp. 1852-1853, 1997.
36. A. Cros, H. Angerer, O. Ambacher, M. Stutzmann, R. Höpler, and T. Metzger, "Raman study of the optical phonons in $Al_xGa_{1-x}N$ alloys", *Solid State Commun.* **104**, pp. 35-39, 1997.
37. F. Demangeot, J. Groenen, J. Frandon, M.A. Renucci, O. Briot, S. Ruffenach-Clur, R.L. Aulombard, "Raman study of $Ga_{1-x}Al_xN$ solid solutions", *MRS Internet J. Nitride Semicond. Res.* **2**, art. 40, 1997.
38. H.S. Loka, S.D. Benjamin, and P.W.E. Smith, "Optical characterization of low-temperature-grown GaAs for ultrafast all-optical switching devices", *IEEE J. Quantum Electron.* **34**, pp. 1426-1437, 1998, and references therein.
39. S. Ruffenach-Clur, O. Briot, J.L. Rouviere, B. Gil, and R.L. Aulombard, "MOVPE growth and characterization of $Al_xGa_{1-x}N$", *Mater. Sci. Eng. B* **50**, pp. 219-222, 1997.
40. L.H. Robins and D.K. Wickenden, "Spatially resolved luminescence studies of defects and stress in aluminum gallium nitride films", *Appl. Phys. Lett.* **71**, pp.3841-3843, 1997.